



HAL
open science

Unexpectedly rapid aerosol formation in the Hunga Tonga plume

Elizabeth Asher, Michael Todt, Karen Rosenlof, Troy Thornberry, Ru-Shan Gao, Ghassan Taha, Paul Walter, Sergio Alvarez, James Flynn, Sean Davis, et al.

► **To cite this version:**

Elizabeth Asher, Michael Todt, Karen Rosenlof, Troy Thornberry, Ru-Shan Gao, et al.. Unexpectedly rapid aerosol formation in the Hunga Tonga plume. *Proceedings of the National Academy of Sciences of the United States of America*, 2023, 120 (46), 10.1073/pnas.2219547120 . hal-04301363

HAL Id: hal-04301363

<https://hal.univ-reunion.fr/hal-04301363>

Submitted on 24 Nov 2023

HAL is a multi-disciplinary open access archive for the deposit and dissemination of scientific research documents, whether they are published or not. The documents may come from teaching and research institutions in France or abroad, or from public or private research centers.

L'archive ouverte pluridisciplinaire **HAL**, est destinée au dépôt et à la diffusion de documents scientifiques de niveau recherche, publiés ou non, émanant des établissements d'enseignement et de recherche français ou étrangers, des laboratoires publics ou privés.

Unexpectedly rapid aerosol formation in the Hunga Tonga plume

Elizabeth Asher^{1,2a*}, Michael Todt^{1,2b}, Karen Rosenlof², Troy Thornberry², RuShan Gao², Ghassan Taha^{3,4}, Paul Walter⁵, Sergio Alvarez⁶, James Flynn⁶, Sean Davis², Stephanie Evan⁷, Jerome Brioude⁷, Jean-Marc Metzger⁸, Dale F. Hurst^{1,9}, Emrys Hall^{1,9}, Kensy Xiong^{1,9}

Elizabeth Asher easher@noaa.gov

Michael Todt michael.todt@colorado.edu

Karen Rosenlof karen.h.rosenlof@noaa.gov

Troy Thornberry troy.thornberry@noaa.gov

RuShan Gao rushan.gao@noaa.gov

Ghassan Taha ghassan.taha-1@nasa.gov

Paul Walter pauljw@stedwards.edu

Sergio Alvarez slalvare@central.uh.edu

James Flynn jhflynn@central.uh.edu

Sean Davis Sean.M.Davis@noaa.gov

Stephanie Evan stephanie.evan@univ-reunion.fr

Jerome Brioude jerome.brioude@univ-reunion.fr

Jean-Marc Metzger jean-marc.metzger@univ-reunion.fr

Dale F. Hurst dale.hurst@noaa.gov

Emrys Hall Emrys.Hall@noaa.gov

Kensy Xiong kensy.xiong@noaa.gov

¹ Cooperative Institute for Research in Environmental Sciences, University of Colorado Boulder, 216 UCB, Boulder, CO 80309, United States

² NOAA Chemical Sciences Laboratory, 325 Broadway, Boulder, CO 80305, United States

³ Morgan State University, 1700 East Cold Spring Lane McMechen Hall Rm 635, Baltimore, MD 21251, United States

⁴ NASA Goddard Space Flight Center, 8800 Greenbelt Rd, Greenbelt, MD 20771, United States

⁵ St. Edward's University, 3001 South congress, Austin, TX 78704, United States

⁶ University of Houston, 4800 Calhoun Rd, Houston, TX 77004, United States

⁷ Laboratoire de l'Atmosphère et des Cyclones (LACy), UMR8105, CNRS, Université de La Réunion, Saint-Denis, France

⁸ Observatoire des Sciences de l'Univers de la Réunion, UAR 3365 (CNRS, Université de la Réunion, Météo-France), Saint-Denis, France

⁹ NOAA Global Monitoring Laboratory, 325 Broadway, Boulder, CO 80305, United States

^a Now at: NOAA Global Monitoring Laboratory

^b Now at: Finnish Meteorological Institute (FMI), Helsinki, Finland

*Corresponding author

Classification: Physical Sciences, Atmospheric Sciences

Keywords: stratospheric aerosol, rapid aerosol formation, SO₂, volcanic plume, Hunga Tonga eruption

47 **Abstract**

48 The Hunga Tonga-Hunga Ha'apai (HT-HH) volcanic eruptions on Jan. 13 and 15, 2022
49 produced a plume with the highest signal in stratospheric aerosol optical depth observed since
50 the eruption of Mt. Pinatubo in 1991. Suites of balloon-borne instruments on a series of launches
51 from Réunion Island intercepted the HT-HH plume within two weeks of the eruptions, yielding
52 observations of the aerosol number and size distribution, and sulfur dioxide (SO₂) and water
53 vapor (H₂O) concentrations. The measurements reveal an unexpected abundance of large
54 particles in the plume, constrain the total sulfur injected to approximately 0.20 Tg, provide
55 information on the altitude of the injection, and indicate that the formation of sulfuric acid
56 aerosol was complete within three weeks. Large H₂O enhancements contributed as much as
57 ~30% to ambient aerosol surface area and likely accelerated SO₂ oxidation and aerosol formation
58 rates in the plume to ~ 3 times faster than under normal stratospheric conditions.
59

60 **Significance Statement**

61 Large volcanic eruptions can play an important role in Earth's radiative balance through
62 stratospheric injections of sulfur dioxide that form sulfate aerosol. Here, we show that in situ
63 observations are critical to constrain the injection mass of stratospheric sulfur and the
64 stratospheric lifetime of sulfur dioxide. Such information is needed to better represent aerosol
65 microphysics and improve predictions of the impacts of natural (or potentially anthropogenic)
66 sulfur dioxide injections. Measurements in the fresh volcanic Hunga Tonga-Hunga Ha'apai
67 plume in January 2022 revealed that stratospheric aerosol formation ended ~3 times faster than is
68 typical in the presence of a large amount of water vapor, resulting in a high signal in aerosol
69 extinction from an abundance of large particles.
70
71
72

73 **Main**

74 Volcanic plumes that reach the stratosphere can influence Earth's radiative balance and
75 are a significant driver of climate variability (1). Under background conditions, sustaining the
76 stratospheric aerosol burden requires the addition of ~ 0.1 Tg sulfur (S) yr^{-1} from the oxidation of
77 carbonyl sulfide and sulfur dioxide (SO_2) (2), while stratospheric transport (3) and a variety of
78 localized aerosol processes (4) contribute to heterogeneity in aerosol number and size.
79 Simulating an eruption's impact on stratospheric aerosol requires either knowledge or
80 assumptions of its injection height and mass (5), plume composition, location, and atmospheric
81 state. In situ measurements within one to three weeks of an eruption can provide critical
82 information for improving these assumptions.

83 The energetic eruption of the underwater Hunga Tonga-Hunga Ha'apai (HT-HH) volcano
84 (20.54°S , 175.38°W) on Jan. 15 (04:00 UTC) (6), together with a smaller eruption on Jan. 13
85 (15:20 UTC), injected an estimated 150 Tg water vapor (H_2O) (7) and 0.41 ± 0.01 Tg SO_2 into
86 the stratosphere (7, 8). The combination of its explosivity and the extraordinary amount of H_2O
87 injected into the stratosphere make the Jan. 15 eruption unique in the satellite era. Estimated
88 injection heights for these two eruptions ranged from 20 km on Jan. 13 to > 30 km on Jan. 15,
89 and the SO_2 plumes quickly overlapped, making them difficult to distinguish (8). Radiosonde
90 measurements reveal enhanced H_2O between 19 km and the maximum altitude of balloon
91 soundings, near 30 km (9). The HT-HH aerosol layer generated the highest signal in
92 stratospheric aerosol optical extinction since the eruption of Mt. Pinatubo in 1991 (10). Given the
93 relatively small injections of SO_2 (7, 8) by the HT-HH eruptions, the large signal in aerosol
94 extinction sparked questions regarding the initial S injection (11), the role of H_2O in rapid
95 aerosol formation in this plume and its timeline (12, 13).

96 In situ observations of particle number concentration and size distribution complement
97 space-based aerosol retrievals. For the first three months after the HT-HH eruption, the Ozone
98 Mapping and Profiler Suite-Limb Profile (OMPS-LP) sensor onboard the Suomi National Polar-
99 orbiting Partnership (S-NPP) satellite supplied a continuous global record of the main volcanic
100 plume's altitude between 16 – 30 km, its horizontal extent and its impact on stratospheric aerosol
101 optical depth (sAOD) (10). The Tonga volcano Rapid Response Experiment (TR^2Ex) provided
102 high-resolution vertical profiles with relatively low uncertainty of SO_2 (14) and H_2O (15, 16) to
103 ~ 30 km altitude and information on the aerosol size distribution in the main plume, which
104 cannot be reliably inferred from either satellite or ground-based measurements. Here, we
105 leverage a combination of these in situ measurements and OMPS-LP retrievals (17) to address
106 questions regarding the HT-HH eruption's impact on the lifetime of SO_2 and the magnitude and
107 altitude of the initial sulfur injection.

108

109

110 **Results**

111 1. Rapid Response Insights

112 TR^2Ex was a unique deployment of a suite of balloon-borne instrumentation that
113 repeatedly analyzed the composition of the volcanic plume 7 – 10 days after the second, larger
114 HT-HH eruption. Sampling the fresh HT-HH plume yielded in situ observations of aerosol size
115 distribution, SO_2 , and H_2O at several pivotal times during its evolution (see Methods, Section 1
116 for details; Table S1). In situ measurements from this campaign allow us to quantify the S
117 gas/particle phase partitioning within the plume, study the vertical distribution of the S injection,

118 and explore the role of stratospheric H₂O enhancements in increasing ambient aerosol size and
119 extinction.

120 Portable Optical Particle Spectrometer (POPS) (18) measurements during TR²Ex show
121 the impact of the HT-HH eruption on aerosol dry mass and extinction (enhancements ranged
122 from two to three orders of magnitude), driven by high concentrations of large accumulation
123 mode aerosols in the volcanic plume (Fig. 1; see Methods, Section 2 for details). By the time the
124 plume reached La Réunion seven days after the second eruption, wind shear had stretched the
125 initial injection into a thin slanted layer of varying thickness as it moved west (19). Positive
126 altitude gradients in easterly windspeeds resulted in progressively shorter transit times with
127 increasing altitude. TR²Ex instruments were unable to measure two isolated optically thin
128 volcanic aerosol layer segments detected above 30 km by space-based and ground-based remote
129 sensing instruments (10, 19)— as these were above the operation ceiling of balloon sondes. Parts
130 of the aerosol layer between 25 km and 28 km (Fig. 1c-d) corresponded to a region with a
131 substantial H₂O enhancement (Fig. S1). Particle number concentration of both large and small
132 particles (up to 1.5 μm) was as much as three orders of magnitude higher than in unperturbed air
133 masses. The mode of the size distribution occurred at ~ 560 nm diameter, and the aerosol
134 effective radius exceeded 0.3 μm (Fig. S2). With H₂O enhancements of ~340 ppmv in this part
135 of the plume, H₂O contributed ~ 15% to the aerosol diameter at ~ 560 nm and ~ 30% to the total
136 aerosol surface area (Fig. S3; see Methods, Section 2). Differences in aerosol surface area impact
137 both extinction and stratospheric chemistry (20), highlighting the importance of calculating
138 ambient aerosol size related to the HT-HH eruption. The air was much drier (< 17 ppmv H₂O) in
139 the part of the plume below 25 km, which contained an elevated number concentration of
140 particles < 700 nm in diameter. The highest number concentration below 25 km occurred at the
141 smallest particle size (Fig. 1e-f), and the aerosol effective radius was not noticeably different
142 from baseline values (~ 0.2 μm; Fig. S2). Larger particles appeared more often in the wetter,
143 higher altitude parts of the aerosol layer, presumably due to shorter SO₂ lifetimes and particle
144 coagulation within the plume (12).

145 On three occasions, simultaneous in situ measurements of SO₂ and aerosol in the volcanic
146 plume reveal varying rates of aerosol formation. Particles in the plume are presumed to be
147 composed of sulfuric acid (H₂SO₄) formed from SO₂ oxidation and are designated estimated
148 H₂SO₄ (eH₂SO₄) (see Methods, Section 2 for details). Comparisons are shown between the mass
149 mixing ratios of S in eH₂SO₄ and SO₂ (Fig. 2a-c). The altitudes of SO₂ enhancements and aerosol
150 accumulations correspond well, and the mass mixing ratios of S in eH₂SO₄ exceeded those of S
151 in SO₂ on two of three flights. Outside of the fresh HT-HH plume, the SO₂ partial pressure was
152 below the detection limit of the SO₂ sonde. If SO₂ gas phase oxidation had proceeded at its
153 typical rate (i.e., an e-folding stratospheric lifetime, τ_{strat} = ~ 30 days) (21) after the two HT-HH
154 eruptions, we would expect a ≤30% estimated H₂SO₄ (eH₂SO₄) aerosol to ≥70% SO₂ split (by S
155 mass) on Jan. 25, ~ 10.5 days after the second, larger eruption. In the wetter, higher altitude
156 region of the plume, measured on Jan. 22, eH₂SO₄ aerosol accounted for 90% of the total S in the
157 plume (Fig. 2d), implying a τ_{strat} = ~ 3 days. In a drier part of the aerosol layer encountered on
158 Jan. 24 at 22 km, eH₂SO₄ aerosol constituted 68% of the total S (τ_{strat} = ~ 8 days), and on Jan. 25
159 at 20 km, only 35% of the total S (τ_{strat} = ~ 24 days). We infer that SO₂ oxidation in the fresh
160 plume proceeded at different rates as a function of H₂O, namely more quickly where H₂O mixing
161 ratios were higher due to an increased concentration of hydroxyl radicals (22, 23). These
162 measurements also provide information on the vertical distribution of the S injection (i.e., the
163 sum of the S in both SO₂ and in eH₂SO₄ aerosol; Fig. 2d). The total S column mass of the higher

164 altitude part of the plume measured on Jan. 22 was nearly four times that of the lower altitude
165 part of the plume measured on Jan. 24 and 25, suggesting that the majority of SO₂ was injected
166 above 25 km (Fig. 2d).

167 168 2. Aerosol burden and stratospheric lifetime (τ_{strat}) of SO₂

169 Quantifying the S burden in the tropical HT-HH aerosol layer helps constrain the
170 stratospheric S injection and the τ_{strat} of SO₂, which are critical for model validation and have
171 widespread implications for stratospheric chemistry. The calculation relies on the relationship
172 between the aerosol S column and sAOD calculated using POPS size distributions on launches
173 from La Réunion and on OMPS-LP retrievals of sAOD (see Methods, Section 3). As the plume
174 moved westwards, TR²Ex launches sampled its core on Jan. 22 – 23 and trailing edge on Jan. 24
175 – 25 (Fig. 3). The S in the eH₂SO₄ aerosol layer grew from 0.03 Tg S on Jan. 18 to 0.15 Tg S on
176 Jan. 26 and reached a maximum of 0.18 Tg S on Feb. 3 (Fig. 4a). We estimate that on Jan. 23, ~
177 3/4 of the S mass was located in the higher altitude part of the aerosol layer, west of La Réunion
178 (Fig. 4a; Methods, Section 3). Leading up to the eruptions (i.e., on Jan. 10), the S burden in
179 background eH₂SO₄ aerosol was < 0.001 Tg S. This result suggests that rapid aerosol conversion
180 took place: within ~ 19 days, all the SO₂ released from the eruptions, corresponding to as much
181 as 0.18 Tg S (8), was oxidized and converted to particles (≥ 140 nm). By tracking the
182 accumulation of S in eH₂SO₄ aerosol, we calculate the average τ_{strat} as ~ 10 – 13 days in the plume
183 (see Methods, Section 4; Fig. 4b). We note, however, that if a sizeable fraction (e.g., 0.09 Tg) of
184 the aerosol mass were not composed of H₂SO₄, this would yield a longer estimated τ_{strat} (~ 14 –
185 17 days) given the same SO₂ injection. A short τ_{strat} , compared with the typical value of one
186 month under climatological stratospheric conditions, helps explain the rapid production of large
187 particles in the HT-HH plume and signals greater availability of the hydroxyl radical to react
188 with methane and trace gases in the stratosphere (12, 22, 23).

189 190 **Discussion**

191 A rapid response to large or unusual volcanic eruptions with in situ observations can
192 provide insight into the resulting aerosol microphysics, complement space-based aerosol
193 retrievals (7, 8, 10), and be essential to evaluate models. Together with satellite retrievals of
194 sAOD, POPS vertical profiles of particle size distributions enable the calculation of the aerosol
195 layer's S mass and the mean τ_{strat} of SO₂. We determined that eH₂SO₄ formation was complete
196 within three weeks, which is consistent with a maximum effective radius (> 0.4 μm) observed in
197 early February (Fig. S2). In situ measurements of SO₂ and eH₂SO₄ and calculations of the aerosol
198 layer's eH₂SO₄ mass provide evidence that the bulk of the total S was injected above 25 km,
199 which cannot be easily deduced from satellite retrievals of SO₂ and aerosol extinction (8, 10).
200 These observations also indicate that SO₂ oxidation and aerosol conversion occurred at varying
201 rates within the plume, corresponding to localized H₂O enhancements. Radiosonde
202 measurements confirm that H₂O mixing ratios within the plume spanned more than an order of
203 magnitude (< 100 ppmv to > 1000 ppmv) (9). Climatological lower stratospheric mixing ratios in
204 the tropics do not typically exceed 4-5 ppmv (24). SO₂ oxidation and aerosol conversion took
205 place ~ 3 times faster, on average, than under climatological stratospheric conditions. SO₂
206 oxidation accelerates substantially in the presence of H₂O enhancements (12, 22, 23, 25). A short
207 τ_{strat} of SO₂ reflects the heightened oxidative capacity of the atmosphere, with important
208 implications on stratospheric chemistry and composition.

209 Our measurements clarify the contributions to aerosol extinction from H₂O after the HT-
210 HH eruptions, which has spurred discussion in the scientific community (10–13). We caution
211 against conflating a response in the aerosol extinction with a similar change in aerosol mass for
212 two reasons: H₂O contributed ~30% to aerosol extinction in the fresh HT-HH plume. Light
213 scattering efficiency is closely related to aerosol size, with a maximum efficiency (per unit
214 volume) at 500 nm diameter (20). Due to the 560 nm diameter mode of the measured aerosol size
215 distribution mode, the HT-HH aerosol layer resulted in a high sAOD relative to its injected mass.
216 Radiosonde measurements show similarly elevated H₂O throughout the plume between Jan. 20
217 and Feb. 1 (one quarter of the observations between 26 – 28 km altitude from all vertical profiles
218 during this period had $7 \leq \text{H}_2\text{O} \leq 130$ ppmv) (26), signifying widespread implications for
219 H_2SO_4 particle size and the S mass in the higher altitude part of the aerosol layer. Particle size
220 distributions show that differences in the peak and shape of the size distribution result in
221 substantial differences in aerosol extinction (e.g., Fig. 1). Questions remain about how H₂O and
222 other compounds reaching the stratosphere during an eruption might influence aerosol
223 microphysics, including the propensity for new particle formation, condensation onto existing
224 particles, and particle coagulation.

225 TR²Ex serves as a roadmap for future rapid response campaigns to volcanic eruptions and
226 other stratospheric perturbations. Campaigns such as TR²EX further the understanding of aerosol
227 processes in the stratosphere and inform models predicting climate impacts under a variety of
228 past and potential future conditions. Stratospheric aerosol injection (SAI), one proposed method
229 of climate intervention, would entail a large anthropogenic addition of stratospheric aerosol. The
230 suite of instruments described here is capable of identifying potential SAI implementations,
231 providing insight into the aerosol composition (i.e., sulfate or other) and hygroscopic effect, and
232 could enable quantifying the mass (and altitude) of SAI.

233

234 **Methods**

235 1. Rapid Response Overview

236 POPS in situ observations (18) of aerosol size distributions were made as part of the
237 National Oceanic and Atmospheric Administration (NOAA) Earth Radiation Budget program's
238 Baseline Balloon Stratospheric Aerosol Profiles (B²SAP) project (27). The B²SAP project
239 combines intensive periods of operation (IOP) with routine baseline measurements in the
240 northern and southern hemispheres. For the Tonga volcano Rapid Response Experiment (TR²Ex)
241 between Jan. 21 and Jan. 26, B²SAP IOP activities were coordinated with additional sonde and
242 lidar measurements at the Maïdo Observatory (28) on La Réunion (21 °S, 55 °E). TR²Ex balloon
243 payloads consisted of either: (A) a POPS, a sulfur dioxide (SO₂) sonde, an Electrochemical
244 Concentration Cell (ECC) ozonesonde and a radiosonde, or (B), an ECC ozonesonde, a Compact
245 Optical Back-scatter Aerosol Detector (COBALD) instrument and a radiosonde (Table S1;
246 COBALD, ozonesonde, and lidar measurements are discussed elsewhere (19). The ground-based
247 lidars and the COBALD provided information on aerosol extinction (18) and backscattering,
248 respectively. Unfortunately, quantitative information on the aerosol depolarization in the plume
249 during TR²Ex does not exist because the lidar at the Maïdo observatory was not calibrated for
250 depolarization. Subsequent POPS and NOAA Frost point Hygrometer (FPH) launches in
251 February, March, and June 2022 at the Maïdo Observatory were part of what are now routine
252 B²SAP soundings (Table S1) (27).

253 SO₂ sonde (14) measurements have lower uncertainty and considerably better vertical
254 resolution than satellite SO₂ retrievals (8), particularly after an energetic volcanic eruption. A

255 modified ECC ozonesonde, the SO₂ sonde removes ozone from the sample prior to detection
256 using a filter, allowing stratospheric as well as tropospheric SO₂ to be quantified using pre-flight
257 calibrations (14). The SO₂ sonde has a ~ 25 sec response time, similar to that of an ozonesonde.
258 SO₂ data (Fig. 2) reflect a correction for this time (and altitude) lag (29, 30). CFH (31) and FPH
259 (16) instruments measuring H₂O were used to calculate ambient particle size, and Ozone
260 Mapping and Profiler Suite-Limb Profile (OMPS-LP) retrievals (17) were used to calculate the
261 volcanic plume's aerosol burden, as described below.
262

263 2. The POPS measurements and inherent assumptions

264 Particle sizing inherently requires assumptions about particle morphology and refractive
265 index related to aerosol composition (18). Here, we assume that particles are spherical and
266 composed of sulfuric acid (H₂SO₄) and water, with a corresponding refractive index of 1.45 at
267 405 nm (the wavelength of the POPS laser), leading to a reported particle number and size
268 distribution between 140 nm – 2.5 μm in diameter. Telemetered data are quality assured based
269 on available engineering parameters, including the instrument temperature, measured with a
270 thermistor located on the POPS laminar flow element, and the instrument flow (27). Particles are
271 expected to be at (or close to) equilibrium with the instrument temperature at the time of
272 detection, given a particle transit time of 60 – 90 ms. We note that POPS particle transit times
273 exceeded modeled timescales required for aerosol growth or evaporation within the plume, in
274 line with similar calculations from Kovilakam and Deshler (32) and Jonsson et al. (33).

275 The S in the eH₂SO₄ aerosol column mass and mass mixing ratios are calculated from the
276 measured aerosol size distribution and particle density. The aerosol weight (wt.%) eH₂SO₄ can be
277 determined using the partial pressure of H₂O at a range of temperatures (34–37). We apply the
278 formulation of Tabazedah et al. (37), which is suitable for low temperatures observed in the
279 lower stratosphere (when eH₂SO₄ ≤ 80 wt. %) and is based on Steele and Hamill (35), and the
280 expression of Gmitro and Vermeulen when eH₂SO₄ > 80 wt. % (34). In the stratosphere,
281 particles have a calculated ≥ 80% wt% eH₂SO₄ at the time of detection due to instrument
282 temperatures (268 – 278 K) that are considerably higher than ambient stratospheric air (ΔT = 50
283 – 75 K). Particle density at the time of detection is both wt.% and temperature dependent (38–
284 40). We use two parameterizations valid for temperatures between 233 – 298 K given different
285 wt. % (39, 40).

286 Ambient particle diameter is calculated according to Steele and Hamill (35) from the
287 measured (dehydrated) particle diameter, the particle wt. % and density both at the time of
288 detection and in ambient air, assuming that the particle was at equilibrium in both cases, and that
289 only water (not H₂SO₄) was lost from the particle during sampling (Fig. S2a). Measured aerosol
290 size distributions were averaged into 100 m altitude bins, to improve counting statistics and
291 facilitate the requisite merges with frost point hygrometer data from other launches. Possible
292 errors in measured particle sizing are driven primarily by Mie resonances (18). Uncertainty in
293 H₂O (<=6%), air temperature (< 1%), and uncertainties in the parameterizations of the wt. % and
294 density contribute additionally to possible errors in calculated ambient sizing (Fig. S2), and the
295 calculated S in eH₂SO₄ mass mixing ratios and column mass (Fig. 2).

296 As in situ size distribution measurements provide no information on aerosol composition,
297 we cannot rule out the possibility that aerosol could have consisted of ash or some other material,
298 such as sea salt, coated (or internally mixed) with H₂SO₄. Contributions from HNO₃ aerosol or
299 mixtures containing HNO₃ and H₂SO₄ were considered but dismissed based on equilibrium
300 calculations (33, 41, 42). Although volcanic lightning on Jan. 15 (43) may have injected NO

301 directly into the stratosphere, HNO_3 hardly condenses at temperatures ≥ 220 K observed in the
302 plume, despite large enhancements in stratospheric H_2O .

303 The assumptions made here regarding particle composition and morphology are
304 supported by space-based Cloud-Aerosol Lidar with Orthogonal Polarization (CALIOP)
305 retrievals and geostationary satellite RGB-Ash composite imagery within the first few days of
306 the HT-HH eruption on Jan. 15 (11). CALIOP retrievals showed particles with low
307 depolarization, indicating spherical H_2SO_4 particles moving westward towards La Réunion on
308 Jan. 20. The geostationary satellite RGB-Ash composite images depicted a concomitant light
309 green SO_2 plume (with little to no ash) during this period.

310

311 3. Calculating the aerosol column and plume S burden

312 Vertical profiles of aerosol extinction at 997 nm, corresponding to the native wavelength
313 of the OMPS-LP sensor, are calculated using publicly available Mie codes (44, 45) and the
314 calculated particle size distribution in ambient air. POPS stratospheric ambient aerosol optical
315 depth (sAOD) is the sum of calculated ambient aerosol extinction above the tropopause.
316 Similarly, the POPS stratospheric S column in eH_2SO_4 aerosol (g S m^{-2}) at a single geographic
317 location is quantified as the sum of the S in eH_2SO_4 aerosol ($\mu\text{g S m}^{-2}$ air) in each 100 m altitude
318 bin above the tropopause. A baseline value of the S column in eH_2SO_4 aerosol, calculated from a
319 vertical profile outside the plume on Jan. 23 (14 UTC), was subtracted from each measurement
320 that encountered the plume to determine the S in the aerosol layer (g S m^{-2}). Because SO_2
321 measurements were below the SO_2 sonde's limit of detection outside the plume, no similar
322 subtraction of the S column in SO_2 under baseline conditions was made following integration for
323 comparisons in Figure 2d.

324 A linear regression between the POPS calculated ambient sAOD and S in eH_2SO_4 column
325 mass enables global retrievals of OMPS-LP sAOD to be used to infer the S column mass across
326 the entire aerosol layer and track the S aerosol burden as the plume evolves. Estimates of the
327 eH_2SO_4 aerosol layer mass, based on relationships between the POPS measured (dehydrated)
328 sAOD and POPS stratospheric S column (\pm uncertainty) and the calculated ambient sAOD and
329 POPS stratospheric S column (\pm uncertainty) over La Réunion between Jan. 22 and Jun. 9 are
330 shown in Figure S4a. The reported uncertainty in OMPS-LP sAOD signal in the stratosphere
331 (10% at $\lambda = 997$ nm) (17) is negligible compared to the differences in the slope and intercept
332 POPS sAOD vs. mass relationships (Fig. S4a). We note that recent debate with respect to
333 potential OMPS-LP retrieval biases (46) is beyond the scope of this work but would lead to a
334 lower eH_2SO_4 aerosol layer mass. The maximum value of daily sAOD from the OMPS-LP sensor
335 on Jan. 10 (50°S – 50°N) was used as the sAOD threshold to identify the geographic extent of
336 the tropical HT-HH aerosol layer (Fig. S4b); its median (0.0025) was used as a background
337 sAOD value in the tropics. The linear relationships from Fig. S4a were applied to each daily
338 sAOD value in the aerosol layer to infer the S column (g S m^{-2}) in each (2° latitude x 24°
339 longitude) grid cell. The resulting S column using the relationship between the ambient sAOD
340 and S in eH_2SO_4 column mass is shown in Figure 3. For reference, the H_2O plume extent,
341 calculated from MLS retrieval levels between 10 and 46 hPa using MLS H_2O anomalies between
342 Jan. 21 – Jan. 23 (defined as the median ± 3 x the mean absolute deviation) is also shown in
343 Figure 3c, compared to the aerosol layer.

344 The S column was then multiplied by the area of the corresponding geographic grid cell
345 (m^2) and summed to determine the total stratospheric S burden (Tg S) over that area. By
346 applying the relationships from Fig. S4a to the background sAOD value, multiplied by the

347 aerosol layer's geographic area, we similarly calculated the corresponding S burden under
 348 background conditions in each case. The S burden under background conditions was then
 349 subtracted from the total stratospheric aerosol S burden to yield the volcanic aerosol layer's S
 350 burden \pm uncertainty (Tg S) shown in Figure 4. The uncertainty in the S burden (the shaded
 351 black region) reflects the range of the estimates shown in Figure S4a. The S mass in the upper
 352 part of the plume was approximated as the sum of the S burden (in eH_2SO_4 aerosol) west of La
 353 Réunion (55° E), when the higher altitude part of the aerosol layer was last observed on Jan. 23
 354 00 UTC (Fig. 1d)(19). La Réunion is located near the latitudinal edge (48° E) of two adjacent
 355 OMPS-LP grid-cells. Thus, this estimate represents the arithmetic mean
 356 (\pm the standard deviation) of the S burden in the adjacent OMPS-LP grid cells centered at 36°
 357 E and 60° E (Fig. 4).

358

359 4. Estimating the SO_2 lifetime

360 By monitoring the aerosol loading following an eruption, we can estimate the initial
 361 injection of S and subsequently deduce the stratospheric lifetime (τ_{strat}) of SO_2 . We assume that
 362 all the SO_2 is converted to H_2SO_4 :

363

$$364 \quad 1. \frac{d[\text{H}_2\text{SO}_4]}{dt} = -\frac{d[\text{SO}_2]}{dt}, \text{ and } [\text{SO}_2] = [\text{SO}_2_{t=0}] - ([\text{H}_2\text{SO}_4] - [\text{H}_2\text{SO}_4_{t=0}])$$

365

366 Making these substitutions into the first order rate law $\frac{d[\text{SO}_2]}{[\text{SO}_2]} = -kdt$ and integrating

367 demonstrates that the amount of H_2SO_4 produced depends on the initial injection of SO_2 and on
 368 the background H_2SO_4 burden (together with any initial injection of aerosol) and enables us to
 369 calculate τ_{strat} of SO_2 through linear regression against t (elapsed days since 4:00 UTC on Jan.
 370 15), where k is the slope of the line and $\tau_{\text{strat}} = 1/k$:

371

$$372 \quad 2. \ln \frac{[\text{SO}_2_{t=0}]}{[\text{SO}_2_{t=0}] - ([\text{H}_2\text{SO}_4] - [\text{H}_2\text{SO}_4_{t=0}])} = kt$$

373

374 The initial injection of S, $\text{SO}_2_{t=0}$, is based on satellite retrievals of SO_2 , which are slightly greater
 375 than the maximum accrual of S in eH_2SO_4 aerosol after the eruption (0.190 Tg; Fig. 4a). τ_{strat} was
 376 calculated using a range of values for the initial SO_2 injection (0.195 – 0.215 Tg S in SO_2). Prior
 377 to the eruption (e.g, on Jan. 10), the initial S burden in the aerosol layer is close to zero (0.0005
 378 Tg S in eH_2SO_4), which is used as the value for $\text{H}_2\text{SO}_4_{t=0}$. If as much as 0.09 Tg of aerosol mass
 379 were not composed of H_2SO_4 (0.03 Tg S is in 0.09 Tg eH_2SO_4) this would result in an estimated
 380 τ_{strat} of 15-17 days. Equation 2 ignores a potential time lag required for either particle formation
 381 or aerosol growth through condensation to particle diameter $\geq 0.14 \mu\text{m}$ from H_2SO_4 gas,
 382 considered negligible in this case.

383

384 Data Availability

385 The processed POPS aerosol size distribution data from all launches used in this study
 386 may be found under the supporting data tab for this manuscript at
 387 <https://csl.noaa.gov/projects/b2sap/data.html>, where processed SO_2 and H_2O data from TR²Ex,
 388 and processed daily files of OMPS-LP sAOD and MLS H_2O plume areas and anomalies from 21
 389 hPa are also available. Raw OMPS-LP and MLS H_2O data may be found at

390 https://disc.gsfc.nasa.gov/datasets/OMPS_NPP_LP_L2_AER_DAILY_2/summary and
391 https://disc.gsfc.nasa.gov/datasets/ML2H2O_004/summary?keywords=aura, respectively. Code
392 is publicly available at <https://github.com/elizabethasher/hthhPY>.

393

394 **Funding Information**

395 This work was supported by the National Oceanic and Atmospheric Administration
396 (NOAA) Earth Radiation Budget program. The authors acknowledge the European
397 Communities, the Région Réunion, CNRS, and Université de la Réunion for their support and
398 contributions in the construction phase of the research infrastructure OPAR (Observatoire de
399 Physique de l'Atmosphère de La Réunion, including Maïdo Observatory). OPAR is presently
400 funded by CNRS (INSU), Météo France, and Université de La Réunion and managed by OSU- R
401 (Observatoire des Sciences de l'Univers de La Réunion, UAR 3365). Development,
402 maintenance, and analysis of the OMPS-LP aerosol product are supported by the NASA Earth
403 Science TASNPP (grant # 80NSSC18K0847) and SNPPSP (grant # 80NSSC22K0157)
404 programs. Opinions, findings and conclusions contained herein reflect the authors' views, not
405 those of NOAA.

406

407 **Open Access**

408 An open access license has not been selected.

409

410 **Competing interests**

411 The authors declare no competing financial interests.

412

413 **Materials and Correspondence**

414 Corresponding author, Elizabeth Asher (Elizabeth.asher@noaa.gov) should be contacted
415 with any questions or requests for material.

416

417

418 **References**

419

- 420 1. S. Solomon, *et al.*, The Persistently Variable “Background” Stratospheric Aerosol Layer
421 and Global Climate Change. *Science* **333**, 866–870 (2011).
- 422 2. A. Feinberg, *et al.*, Improved tropospheric and stratospheric sulfur cycle in the aerosol–
423 chemistry–climate model SOCOL-AERv2. *Geosci. Model Dev.* **12**, 3863–3887 (2019).
- 424 3. M. H. Hitchman, M. McKay, C. R. Trepte, A climatology of stratospheric aerosol. *J.*
425 *Geophys. Res.* **99**, 20689 (1994).
- 426 4. S. Kremser, *et al.*, Stratospheric aerosol-Observations, processes, and impact on climate:
427 Stratospheric Aerosol. *Rev. Geophys.* **54**, 278–335 (2016).
- 428 5. L. O. Muser, *et al.*, Particle aging and aerosol–radiation interaction affect volcanic plume
429 dispersion: evidence from the Raikoke 2019 eruption. *Atmospheric Chem. Phys.* **20**, 15015–
430 15036 (2020).

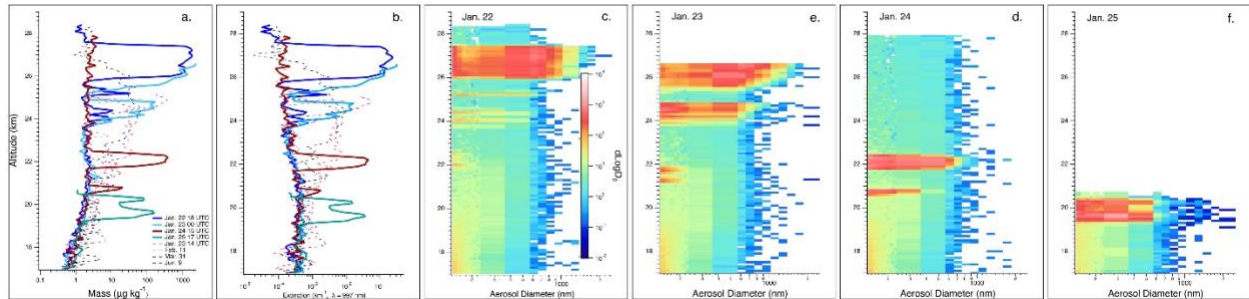
- 431 6. C. J. Wright, *et al.*, Surface-to-space atmospheric waves from Hunga Tonga–Hunga
432 Ha’apai eruption. *Nature* **609**, 741–746 (2022).
- 433 7. L. Millán, *et al.*, The Hunga Tonga-Hunga Ha’apai Hydration of the Stratosphere. *Geophys.*
434 *Res. Lett.* **49** (2022).
- 435 8. S. A. Carn, N. A. Krotkov, B. L. Fisher, C. Li, Out of the blue: Volcanic SO₂ emissions
436 during the 2021–2022 eruptions of Hunga Tonga—Hunga Ha’apai (Tonga). *Front. Earth*
437 *Sci.* **10**, 976962 (2022).
- 438 9. H. Vömel, S. Evan, M. Tully, Water vapor injection into the stratosphere by Hunga Tonga-
439 Hunga Ha’apai. *Science* **377**, 1444–1447 (2022).
- 440 10. G. Taha, *et al.*, Tracking the 2022 Hunga Tonga-Hunga Ha’apai aerosol cloud in the upper
441 and middle stratosphere using space-based observations. *Geophys. Res. Lett.* (2022)
442 <https://doi.org/10.1029/2022GL100091> (October 2, 2022).
- 443 11. B. Legras, *et al.*, The evolution and dynamics of the Hunga Tonga–Hunga Ha’apai sulfate
444 aerosol plume in the stratosphere. *Atmospheric Chem. Phys.* **22**, 14957–14970 (2022).
- 445 12. Y. Zhu, *et al.*, Perturbations in stratospheric aerosol evolution due to the water-rich plume
446 of the 2022 Hunga-Tonga eruption. *Commun. Earth Environ.* **3**, 248 (2022).
- 447 13. M. R. Schoeberl, *et al.*, Analysis and Impact of the Hunga Tonga-Hunga Ha’apai
448 Stratospheric Water Vapor Plume. *Geophys. Res. Lett.* **49** (2022).
- 449 14. S. Yoon, *et al.*, Development and testing of a novel sulfur dioxide sonde. *Atmospheric*
450 *Meas. Tech.* **15**, 4373–4384 (2022).
- 451 15. H. Vömel, T. Naebert, R. Dirksen, M. Sommer, An update on the uncertainties of water
452 vapor measurements using cryogenic frost point hygrometers. *Atmospheric Meas. Tech.* **9**,
453 3755–3768 (2016).
- 454 16. E. G. Hall, *et al.*, Advancements, measurement uncertainties, and recent comparisons of the
455 NOAA frost point hygrometer. *Atmospheric Meas. Tech.* **9**, 4295–4310 (2016).
- 456 17. G. Taha, *et al.*, OMPS LP Version 2.0 multi-wavelength aerosol extinction coefficient
457 retrieval algorithm. *Atmospheric Meas. Tech.* **14**, 1015–1036 (2021).
- 458 18. R. S. Gao, *et al.*, A light-weight, high-sensitivity particle spectrometer for PM_{2.5} aerosol
459 measurements. *Aerosol Sci. Technol.* **50**, 88–99 (2016).
- 460 19. A. Baron, *et al.*, Early Evolution of the Stratospheric Aerosol Plume Following the 2022
461 Hunga Tonga-Hunga Ha’apai Eruption: Lidar Observations From Reunion (21°S, 55°E).
462 *Geophys. Res. Lett.* **50**, e2022GL101751 (2023).

- 463 20. D. M. Murphy, *et al.*, Radiative and chemical implications of the size and composition of
464 aerosol particles in the existing or modified global stratosphere. *Atmospheric Chem. Phys.*
465 **21**, 8915–8932 (2021).
- 466 21. M. Höpfner, *et al.*, Sulfur dioxide (SO₂) from MIPAS in the upper troposphere and lower
467 stratosphere 2002–2012. *Atmospheric Chem. Phys.* **15**, 7017–7037 (2015).
- 468 22. A. N. LeGrande, K. Tsigaridis, S. E. Bauer, Role of atmospheric chemistry in the climate
469 impacts of stratospheric volcanic injections. *Nat. Geosci.* **9**, 652–655 (2016).
- 470 23. J. H. Seinfeld, Pandis, Spyros N., *Atmospheric Chemistry and Physics: From Air Pollution*
471 *to Climate Change* (John Wiley & Sons, 2006).
- 472 24. D. F. Hurst, *et al.*, Recent divergences in stratospheric water vapor measurements by frost
473 pointhygrometers and the Aura Microwave Limb Sounder. *Atmospheric Meas. Tech.* **9**,
474 4447–4457 (2016).
- 475 25. Y. Zhu, *et al.*, Persisting volcanic ash particles impact stratospheric SO₂ lifetime and
476 aerosol optical properties. *Nat. Commun.* **11**, 4526 (2020).
- 477 26. Vömel, Holger, Hunga Tonga-Hunga Ha’apai stratospheric water vapor from Vaisala RS41
478 radiosondes <https://doi.org/10.5065/P328-Z959> (September 25, 2022).
- 479 27. M. A. Todt, *et al.*, Baseline Balloon Stratospheric Aerosol Profiles (B² SAP)- Systematic
480 measurements of aerosol number density and size. *J. Geophys. Res. Atmospheres*,
481 e2022JD038041 (2023).
- 482 28. A. Baron, *et al.*, “Early evolution of the Hunga – Tonga Volcanic Plume from Lidar
483 Observations at Reunion Island (Indian Ocean, 21°S, 55°E)” (display, 2022)
484 <https://doi.org/10.5194/egusphere-egu22-13599> (February 5, 2023).
- 485 29. H. Vömel, *et al.*, A new method to correct the electrochemical concentration cell (ECC)
486 ozonesonde time response and its implications for “background current” and pump
487 efficiency. *Atmospheric Meas. Tech.* **13**, 5667–5680 (2020).
- 488 30. L.-J. Huang, M.-J. Chen, C.-H. Lai, H.-T. Hsu, C.-H. Lin, New Data Processing Equation to
489 Improve the Response Time of an Electrochemical Concentration Cell (ECC) Ozonesonde.
490 *Aerosol Air Qual. Res.* **15**, 935–944 (2015).
- 491 31. H. Vömel, D. E. David, K. Smith, Accuracy of tropospheric and stratospheric water vapor
492 measurements by the cryogenic frost point hygrometer: Instrumental details and
493 observations. *J. Geophys. Res.* **112**, D08305 (2007).
- 494 32. M. Kovilakam, T. Deshler, On the accuracy of stratospheric aerosol extinction derived from
495 in situ size distribution measurements and surface area density derived from remote SAGE
496 II and HALOE extinction measurements. *J. Geophys. Res. Atmospheres* **120**, 8426–8447
497 (2015).

- 498 33. H. H. Jonsson, *et al.*, Performance of a Focused Cavity Aerosol Spectrometer for
499 Measurements in the Stratosphere of Particle Size in the 0.06–2.0- μm -Diameter Range. *J.*
500 *Atmospheric Ocean. Technol.* **12**, 115–129 (1995).
- 501 34. J. I. Gmitro, T. Vermeulen, Vapor-liquid equilibria for aqueous sulfuric acid. *AIChE J.* **10**,
502 740–746 (1964).
- 503 35. H. M. Steele, P. Hamill, Effects of temperature and humidity on the growth and optical
504 properties of sulphuric acid–water droplets in the stratosphere. *J. Aerosol Sci.* **12**, 517–528
505 (1981).
- 506 36. S. L. Clegg, P. Brimblecombe, Application of a Multicomponent Thermodynamic Model to
507 Activities and Thermal Properties of 0–40 mol kg⁻¹ Aqueous Sulfuric Acid from <200 to
508 328 K. *J. Chem. Eng. Data* **41**, 1530–1530 (1996).
- 509 37. A. Tabazadeh, O. B. Toon, S. L. Clegg, P. Hamill, A new parameterization of H₂SO₄/H₂
510 O aerosol composition: Atmospheric implications. *Geophys. Res. Lett.* **24**, 1931–1934
511 (1997).
- 512 38. E. Washburn W., Ed., *International critical tables of numerical data, physics, chemistry*
513 *and technology* (McGraw-Hill, 1928).
- 514 39. M. Kulmala, A. Laaksonen, L. Pirjola, Parameterizations for sulfuric acid/water nucleation
515 rates. *J. Geophys. Res. Atmospheres* **103**, 8301–8307 (1998).
- 516 40. L. Oca, J. M. Campillo-Robles, M. M. Bou-Ali, Review and Analysis of Thermophysical
517 Properties of a Sulfuric Acid–Water Electrolyte. *J. Chem. Eng. Data* **63**, 3572–3583 (2018).
- 518 41. M. D. Petters, S. M. Kreidenweis, A single parameter representation of hygroscopic growth
519 and cloud condensation nucleus activity. *Atmospheric Chem. Phys.* **7**, 1961–1971 (2007).
- 520 42. Jack Alf Goff, S. Gratch, Low-pressure properties of water from -160 to 212 °F in
521 (Transactions of the American Society of Heating and Ventilating Engineers, 1946), pp.
522 95–122.
- 523 43. D. A. Yuen, *et al.*, Under the surface: Pressure-induced planetary-scale waves, volcanic
524 lightning, and gaseous clouds caused by the submarine eruption of Hunga Tonga-Hunga
525 Ha’apai volcano. *Earthq. Res. Adv.* **2**, 100134 (2022).
- 526 44. C. F. Bohren, D. R. Huffman, *Absorption and Scattering of Light by Small Particles*, 1st
527 Ed. (Wiley, 1998) <https://doi.org/10.1002/9783527618156> (September 23, 2022).
- 528 45. B. J. Sumlin, W. R. Heinson, R. K. Chakrabarty, Retrieving the aerosol complex refractive
529 index using PyMieScatt: A Mie computational package with visualization capabilities. *J.*
530 *Quant. Spectrosc. Radiat. Transf.* **205**, 127–134 (2018).
- 531 46. A. E. Bourassa, *et al.*, Tomographic Retrievals of Hunga Tonga-Hunga Ha’apai Volcanic
532 Aerosol. *Geophys. Res. Lett.* **50** (2023).

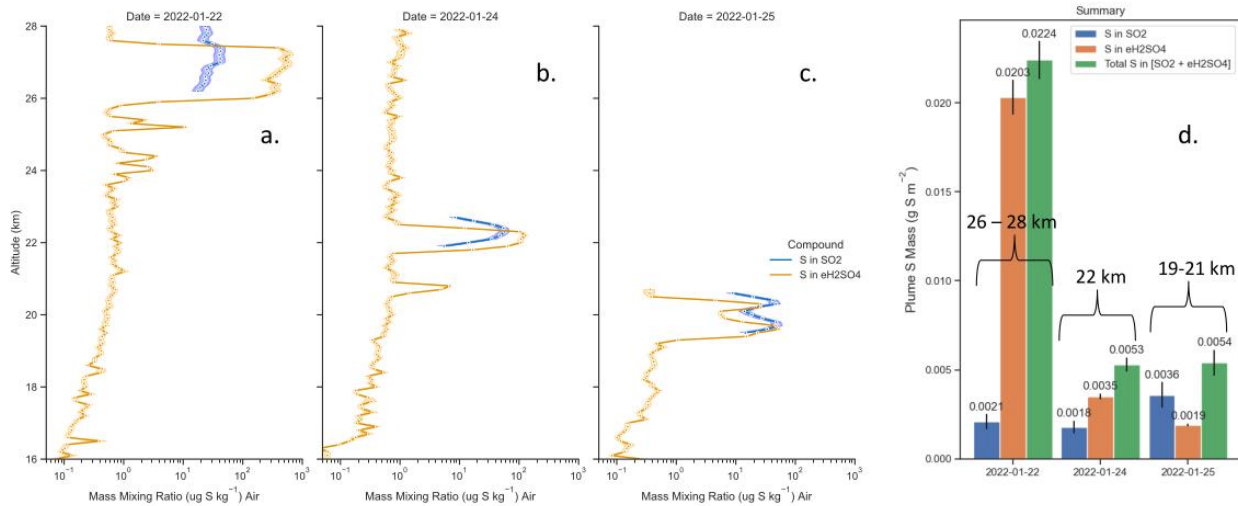
533
534
535
536
537

Figures



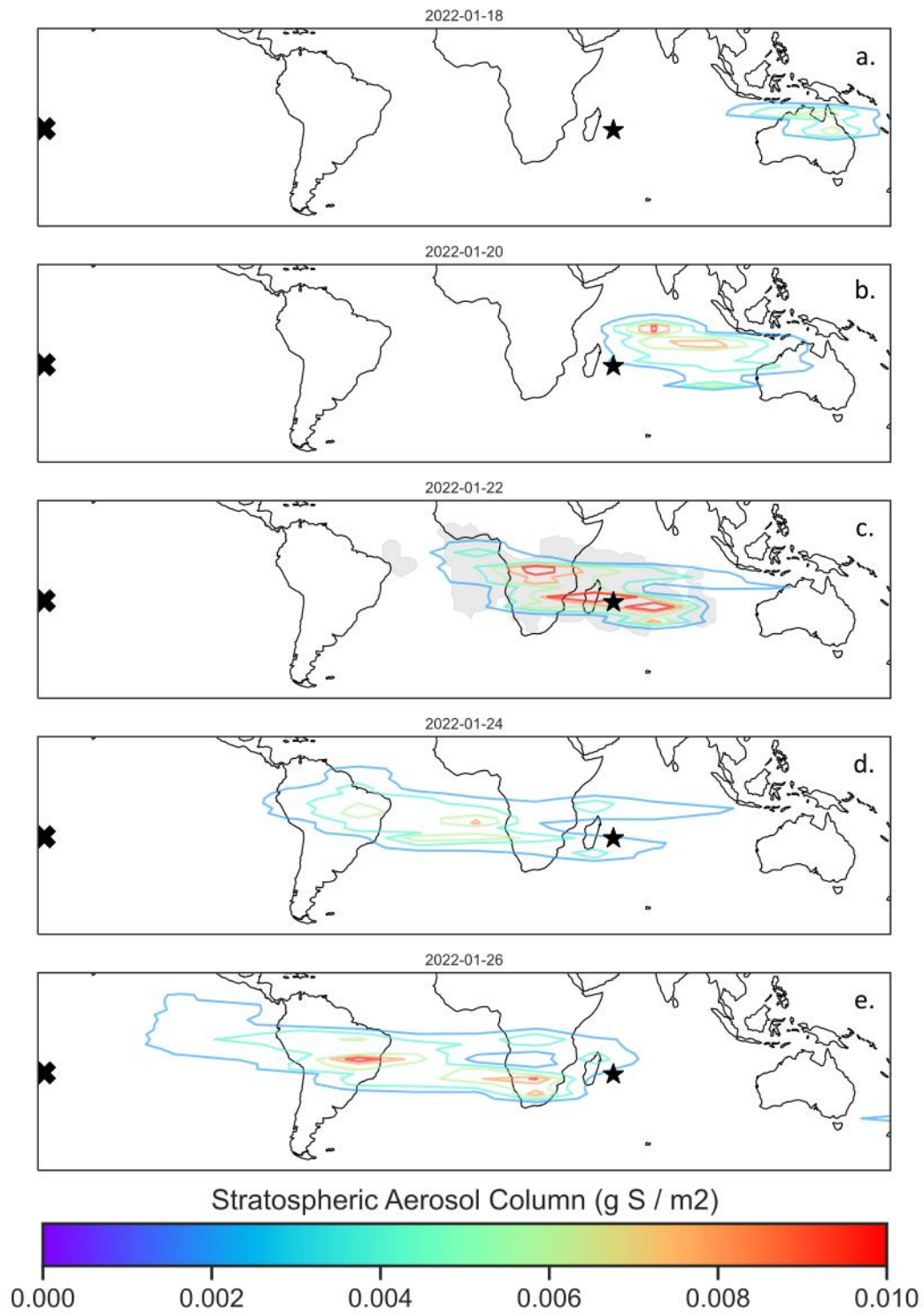
538
539
540
541
542
543
544
545
546

Figure 1. Vertical profiles of calculated bulk aerosol properties between January and June 2022 (from POPS size distribution data), including mass mixing ratios (a) and ambient extinction using Steele and Hamill (35)(b), both of which use the legend in panel (a), and vertical profiles of the measured aerosol size distributions from TR²Ex launches when the fresh HT-HH aerosol plume was encountered (c, d, e, f). Aerosol size distributions (dN/dLogD_p) for the four TR²Ex soundings (c, d, e, f) use the color scale in panel (c).



547
548
549
550
551
552
553
554

Figure 2. On three different dates, vertical profiles of S in SO₂ mass mixing ratios and calculated S in eH₂SO₄ mass mixing ratios based on aerosol size distributions, when both instruments measured the volcanic plume with low uncertainties (a-c), and a summary of the S column mass in SO₂, the S column mass in eH₂SO₄, and the total S column mass ([S in SO₂] + [S in eH₂SO₄]) observed within the plume (d). Shaded areas and error bars show the uncertainty in SO₂ sonde measurements ($\leq 20\%$) and the uncertainty in calculated eH₂SO₄ mass mixing ratios and S mass including possible error related to aerosol sizing and aerosol density.

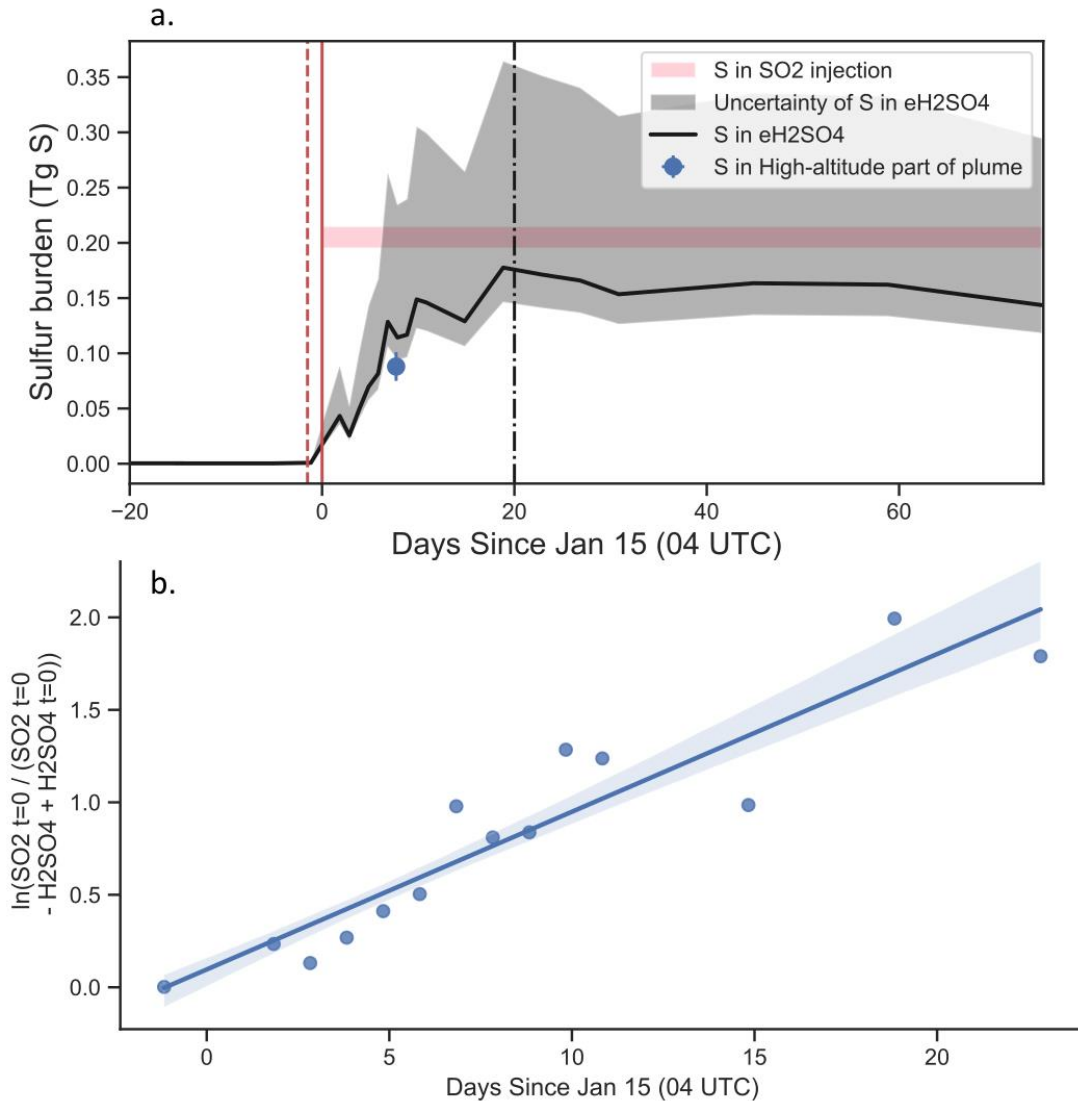


556

557 **Figure 3.** Contour plots of the eH_2SO_4 aerosol column (g m^{-2}), calculated using the equation in

558 the Fig. S4a caption, for 5 days from Jan. 18 to Jan 26 (a-e). On Jan. 22, the gray shaded area

559 shows the maximum plume extent between Jan. 21 – Jan. 23 as determined from MLS H₂O
 560 anomalies at 21 hPa. Locations of HT-HH and La Réunion are marked with a cross and star,
 561 respectively.
 562



563
 564 **Figure 4.** A time series of the calculated S burden in eH₂SO₄ aerosol, calculated using a
 565 combination of POPS measurements and OMPS-LP retrievals (a) and the estimation of the τ_{strat}
 566 (b). The calculated S burden in eH₂SO₄ aerosol (black line) represents the relationship between
 567 calculated ambient sAOD and the mass, and agrees with estimates of the S injected as SO₂ from
 568 satellites (7, 8) (pink shaded region). The uncertainty (black shaded region) represents the range
 569 of assumptions considered in Figure S4a. The approximated S mass in the higher altitude part of
 570 the plume, west of La Réunion on Jan. 23 00 UTC is also shown. OMPS-LP Dashed vertical
 571 lines depict the period of eH₂SO₄ aerosol accumulation. The S burden from this period is used to
 572 calculate the stratospheric lifetime of SO₂, $\tau_{\text{strat}} = 1/k$, as shown in equation 3 (Methods

573 Section 3). Assuming an SO₂ injection of 0.205 Tg S in SO₂ (7, 8) $k = 0.10$ ($r^2 = 0.87$; $p <$
574 $1.23E-6$; 1 standard deviation of the slope is ± 0.011), suggesting a τ_{strat} for SO₂ of ~ 10 days (b).
575